Archival Report

Biological Psychiatry

TAAR1-Dependent and -Independent Actions of Tyramine in Interaction With Glutamate Underlie Central Effects of Monoamine Oxidase Inhibition

Ioannis Mantas, Theodosia Vallianatou, Yunting Yang, Mohammadreza Shariatgorji, Maria Kalomoiri, Elva Fridjonsdottir, Mark J. Millan, Xiaoqun Zhang, Per E. Andrén, and Per Svenningsson

ABSTRACT

BACKGROUND: Monoamine oxidase inhibitors (MAOIs) exert therapeutic actions by elevating extracellular levels of monoamines in the brain. Irreversible MAOIs cause serious hypertensive crises owing to peripheral accumulation of tyramine, but the role of tyramine in the central effects of MAOIs remains elusive, an issue addressed herein. To achieve robust inhibition of MAOA/B, the clinically used antidepressant tranylcypromine (TCP) was employed.

METHODS: Behavioral, histological, mass spectrometry imaging, and biosensor-mediated measures of glutamate were conducted with MAOIs in wild-type and TAAR1-knockout (KO) mice.

RESULTS: Both antidepressant and locomotion responses to TCP were enhanced in TAAR1-KO mice. A recently developed fluoromethylpyridinium-based mass spectrometry imaging method revealed robust accumulation of striatal tyramine on TCP administration. Furthermore, tyramine accumulation was higher in TAAR1-KO versus wild-type mice, suggesting a negative feedback mechanism for TAAR1 in sensing tyramine levels. Combined histoenzymological and immunohistological studies revealed hitherto unknown TAAR1 localization in brain areas projecting to the substantia nigra/ventral tegmental area. Using an enzyme-based biosensor technology, we found that both TCP and tyramine reduced glutamate release in the substantia nigra in wild-type but not in TAAR1-KO mice. Moreover, glutamate measures in freely moving animals treated with TCP demonstrated that TAAR1 prevents glutamate accumulation in the substantia nigra during hyperlocomotive states.

CONCLUSIONS: These observations suggest that tyramine, in interaction with glutamate, is involved in centrally mediated behavioral, transcriptional, and neurochemical effects of MAOIs.

https://doi.org/10.1016/j.biopsych.2020.12.008

Monoamine oxidase (MAO) is a mitochondrial enzyme that plays a pivotal role in the intracellular inactivation of monoaminergic neurotransmitters. MAO inhibitors (MAOIs) have long been used for the treatment of Parkinson's disease, major depressive disorder, and anxiety (1,2). In addition, polymorphisms in MAO genes have been associated with schizophrenia and personality disorders (3–5). There are two MAO enzyme isoforms, MAOA and MAOB, which differ in their substrate specificity: serotonin (5-HT) and norepinephrine (NE) are primarily broken down by MAOA, while dopamine (DA) is degraded by both MAOA and MAOB (2). MAO inhibition results in the accumulation of 5-HT, NE, and DA along with trace amines (TAs), such as tyramine (2).

TAs have low concentration in biological fluids compared with classical monoamines. Parkinson's disease is associated with high tyramine plasma levels, while major depressive disorder displays low urine levels of the same TA (6–9). Tyramine is known to induce monoamine release in an amphetamine-like manner through an interaction with VMAT2 (7,10–12). Tyramine is generated by the AADC (aromatic L-amino acid decarboxylase)–mediated decarboxylation of tyrosine and is mainly colocalized with DA in nigrostriatal neurons (6,7,12). Tyramine can be degraded by both MAO isoforms, but MAOB predominates in dopaminergic pathways. The literature focuses on the fact that MAOI-induced elevations of tyramine mediate severe peripheral side effects (13). The so-called tyramine syndrome in MAOI-treated patients is characterized by a life-threatening elevation of blood pressure after the ingestion of tyramine-rich foods (13). Specifically, the monoamine-releasing properties of tyramine cause an NE efflux from the postganglionic sympathetic nerve terminals (13). There is comparatively sparse knowledge on the regulation and role of tyramine in modulating effects of MAOIs in the brain.

TAARs are GPCRs (G protein–coupled receptors) that belong to the rhodopsin subclass A of the GPCR superfamily

ISSN: 0006-3223

(14,15). There is evidence that TAARs display G_s, G_q, and G_{13} coupling; interestingly, this can occur with the TA localized intracellularly rather than on the surface membrane (16–19). In addition to binding TAs, such as tyramine, TAAR1 is activated by several classes of psychoactive agents employed for both therapeutic and recreational purposes, notably amphetamine, methamphetamine, and MDMA (methylenedioxymethamphetamine) (6,20–22). TAAR1 is expressed in the stomach, pancreas, and, along with TAAR5, in limbic and periventricular areas of the brain (7,14,23). TAAR1 is enriched in monoaminergic perikarya, such as the ventral tegmental area (VTA), substantia nigra pars compacta (SNc), dorsal raphe nucleus, and the nucleus of the solitary tract; it is also present in the prefrontal cortex, entorhinal cortex, hypothalamus, and amygdala (24,25). VTA and dorsal raphe neurons show a robust increase of spontaneous firing after application of the TAAR1 selective antagonist EPPTB and in TAAR1-knockout (KO) mice compared with wild-type (WT) mice, suggesting that TAAR1 exerts an inhibitory tone on the activity of dopaminergic and serotonergic neurons (26–28). Accordingly, TAAR1-KO mice display behavioral hypersensitivity and more pronounced increases in extracellular levels of monoamines in projection regions such as the nucleus accumbens, striatum, and cortex on exposure to psychostimulants (24,27,29). Conversely, agonist stimulation of TAAR1 blunts actions of psychostimulants (27). The above observations underpin interest in TAAR1 as a potential target for novel classes of medication treating depression (antagonists) or psychotic disorders (agonists). Many compounds, both selective and multitarget, have been generated to this end (30), and encouraging observations have been acquired in experimental and clinical studies (31). Most recently, the combined TAAR1/5-HT_{1A} receptor agonist SEP-363856 showed antipsychotic activity in patients with schizophrenia (31,32). Should these observations be corroborated in larger trials, SEP-363856 would become the first non–dopamine D_2 receptor antagonist available for the treatment of schizophrenia (31,32).

Despite the abovementioned observations supporting the physiological, etiological, and therapeutic significance of tyramine and TAAR1s, knowledge remains limited. Previous studies have examined the role of TAAR1 under conditions in which the synthesis and metabolism of tyramine have not been directly perturbed. Here, we decided to examine effects of tyramine and TAAR1 under conditions in which the levels of tyramine are elevated by means of MAO inhibition. Taking advantage of a recently developed fluoromethylpyridinium-based matrix assisted laser desorption/ionization (MALDI) imaging method (33), we visualized and quantified tyramine, along with other monoamines and metabolites, in the striatum of both WT and TAAR1-KO mice, following MAO inhibition. Mice were treated with the nonselective and irreversible MAOI tranylcypromine (TCP), which is not only a tool for MAO inhibition but also clinically used for the management of resistant and atypical depression with motor retardation (34,35). Using multiple methodological approaches, we explored the roles of tyramine and TAAR1 in mediating therapeutically relevant behavioral, transcriptional, and neurochemical actions of TCP.

METHODS AND MATERIALS

Animals

Adult male and female WT and TAAR1-KO animals (29) were housed in temperature- and humidity-controlled rooms (20°C, 53% humidity) with a 12-hour light/dark cycle and access to food pellets and water ad libitum.

Behavioral Tests

Adult male and female mice were randomized according to genotype and treatment and tested by videotracking in the open field test and forced swim test. All behavioral tests were performed during the light cycle by experimenters blinded to the genotype and treatment. The equipment and detailed protocols are described in the Supplement.

Drugs

TCP, clorgiline, and rasagiline mesylate were dissolved in saline solution. Desipramine and pargyline were dissolved in 10% dimethyl sulfoxide solution. These chemicals were purchased from Sigma-Aldrich (St. Louis, MO). Drugs were administered intraperitoneally (i.p.). EPPTB and tyramine (Sigma-Aldrich) were administered locally during fast analytical sensing technology (FAST) recordings of glutamate neurotransmission.

Intrastriatal 6-Hydroxydopamine Lesioning

To selectively denervate nigrostriatal DA neurons, but to protect NE neurons, mice were pretreated with 25 mg/kg desipramine (i.p.; Sigma-Aldrich) and 5 mg/kg pargyline (i.p.; Sigma-Aldrich), anesthetized, placed in a stereotaxic frame, and injected with 1 μL of 6-hydroxydopamine (6-OHDA) solution into the striatum of the right hemisphere. The detailed procedure is described in the Supplement.

MAO Activity Assay

Fresh-frozen forebrain tissue was homogenized and used for isolation of crude mitochondrial fraction. The isolated mitochondrial fraction was used for MAOA and MAOB activity quantification using an Amplex Red Monoamine Oxidase Assay Kit (Thermo Fisher Scientific, Waltham, MA), as detailed in the Supplement.

MALDI–Mass Spectrometry Imaging of Neurotransmitters and Metabolites

Fresh-frozen brain tissue sections collected for MALDI–mass spectrometry imaging (MSI) were thaw-mounted on indium tin oxide–coated glass slides (Bruker Daltonics GmbH, Bremen, Germany). For MALDI-MSI of neurotransmitters and metabolites, on-tissue derivatization was performed according to a previously published protocol (33). For details, see the Supplement.

[^{125}I]-RTI55 Autoradiography to Detect DA Transporter

Fresh-frozen brain sections were processed for autoradiographic detection of DA transporter by [^{125}I]-RTI55 as previously described (36).

In Situ Hybridization Experiments

Fresh-frozen, postfixed brain sections were hybridized with ^{35}S-radiolabeled riboprobes targeting *Arc*, *Pdyn*, *Penk*, or *Ppp1r1b* genes or RNAscope (Advanced Cell Diagnostics, Newark, CA) ZZ-probes targeting *Arc* or *Pdyn*. A detailed description is provided in the Supplement.

X-gal Staining and Immunofluorescence to Detect TAAR1

Perfused, postfixed brain sections were stained for X-gal according to the manufacturer's instructions (Sigma-Aldrich). After the staining, they were immediately subjected to immunofluorescence protocol as described in the Supplement.

In Vivo FAST Recordings of Glutamate

A ceramic-based microelectrode array (Quanteon, Nicholasville, KY) was connected to a microinjector and stereotactically guided to the region of interest as previously described (37–39). The detailed protocol and analysis of the recordings in both anesthetized and freely moving animals is described in the Supplement.

Statistical Analysis

Statistical analysis was carried out by two-/three-way analysis of variance (ANOVA) or two-/three-way repeated-measures (RM) ANOVA followed by Tukey's honestly significant difference post-test. Statistical software for ANOVA, principal component analysis, and partial least squares and plotting graphs are detailed in the Supplement. Supplemental statistical (including *F* statistic, *p* values) tables for each graph are presented in the Supplement.

RESULTS

TAAR1-KO Animals Display Increased Antidepressant and Locomotive Responses to Irreversible MAOA/B Inhibitors

Nonselective MAOIs have an antidepressant effect in the forced swim test (40). The effective antidepressant (i.p.) dose of TCP in WT mice starts from 4 mg/kg (40). To be able to detect any enhanced response in TAAR1-KO mice, we used the subeffective dose of 3 mg/kg. Two-way ANOVA showed that administration of TCP had a significant effect in forced swim test immobility time (Figure 1A, B and Table S1). Post hoc analysis revealed a significant treatment effect only in TAAR1-KO mice. Furthermore, we measured the difference in immobility time of each genotype and found that TAAR1-KO mice showed a significantly larger difference than the WT mice (Figure 1C). Irreversible inhibition of both MAO isoenzymes with either TCP or a combination of MAOA and MAOB inhibitors causes an increase in locomotive activity in mice (35,41,42). We therefore studied the locomotive response of WT and TAAR1-KO mice on TCP administration. To investigate whether the effects of TCP depend on MAO inhibition or could relate to TCP's amphetamine-like structure, we also examined the irreversible selective MAOIs clorgiline (MAOA) and rasagiline (MAOB). A two-way ANOVA showed a significant interaction between genotype and treatment factor (Figure 1D–G and Table S1). Post hoc test showed a significant locomotor increase in both TAAR1-KO and WT mice after the administration of 10 mg/kg of TCP or the combination of 10 mg/kg clorgiline with 3 mg/kg rasagiline (Figure 1D–G). However, neither WT nor TAAR1-KO mice showed any significant effect after treatment with rasagiline or clorgiline alone or after a lower dose of TCP (3 mg/kg) (Figure 1D–G). In conclusion, TAAR1-KO mice show increased behavioral responsivity to nonselective inhibition of MAO.

Striatum Shows Strongly Enhanced Tyramine Levels on Chronic Nonselective MAOA/B Irreversible Treatment With TCP, Particularly in TAAR1-KO Mice

We did not find any significant genotype difference in MAO activity from brain lysates (Figure S1). We therefore explored whether the behavioral genotype difference was dependent on alterations in the levels of tyramine, monoamines, and/or their metabolites. We used a recently developed MALDI-MSI method to quantify tyramine, monoamines, and their metabolites after TCP in WT and TAAR1-KO mice (33). To avoid possible fluctuations of monoamine metabolites after MAO inhibition, we administered TCP chronically (Figure 2A). To ensure that TCP was pharmacologically active, we measured locomotor responses after 2 weeks (Figure 2A). Moreover, to address the role of the nigrostriatal system in regulating TCP-induced changes in monoamines, particularly tyramine, we intrastriatally injected 6-OHDA on the 15th day of the experiment (Figure 2A). Two-way ANOVA indicated significant effects of genotype and treatment factors during the first hour of recording in the open field test after 2 weeks of daily TCP treatment (Figure 2B and Table S2). Post hoc analysis indicated that TAAR1-KO mice were sensitized to a higher degree than their WT counterparts (Figure 2B). Regarding the lesion efficacy, three-way RM ANOVA showed that there was a significant decrease of striatal DA transporter binding in the lesioned side of all studied groups (Figure S2 and Table S3). The same analysis did not show any significant effect of the treatment or the genotype, demonstrating that TCP is not affecting the neurotoxic effect of 6-OHDA in either genotype (Figure S2 and Table S3). Regarding the MSI data, we identified all the previously characterized metabolites (33). We were able to pinpoint the peak of TCP itself, which did not differ significantly between the two genotypes (Figure S3 and Table S4). A small difference between the intact and lesion side may stem from the loss of DA terminals containing the brain-enriched xenobiotic degrading enzyme CYP2D6 (43). Metabolites positioned upstream or downstream of the MAOA/B degrading step were substantially increased or decreased, respectively, while the rest of the metabolites remained unchanged (Figure 2D and Figure S4). We applied an unsupervised data analysis method to acquire a comprehensive view of the data. Briefly, we performed principal component analysis using the root-mean-square fold change of each sample to the average of WT saline intact hemispheres for 26 well-identified peaks in striatal regions of interest. We used this analysis method to identify possible metabolites that contribute to the differentiation of the samples regarding genotype, treatment, and hemisphere factor (Figure 2E, F and Tables S5 and S6). Three-way RM ANOVA using the *t*-score

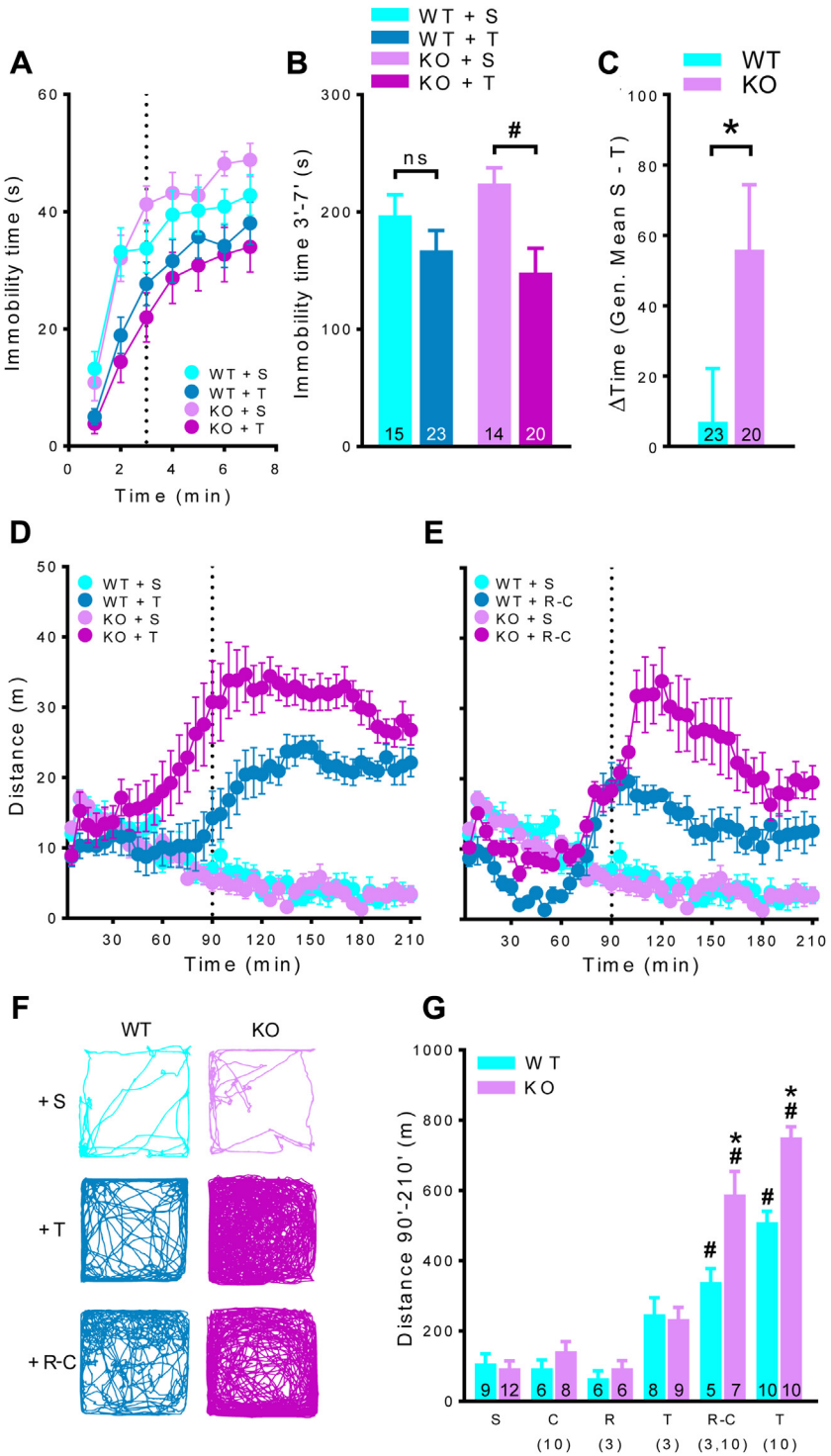

Figure 1. Monoamine oxidase inhibition produces stronger antidepressant and locomotive responses in TAAR1-KO than WT mice. **(A)** Line showing the immobility time in forced swim test in 1-minute time-bins over a period of 7 minutes after the administration of tranylcypromine (3 mg/kg). The intraperitoneal injection was administered 120 minutes before the test. **(B)** Bar graph depicting the immobility time of the different groups during the last 5 minutes of the test. S vs. T, #$p < .05$, Tukey's honestly significant difference. **(C)** Bar graph showing the difference (Δ) between the immobility time of each tranylcypromine-treated animal and the respective genotype mean immobility time of the saline group.*$p < .05$, Student's t test. **(D, E)** Line graphs showing the distance traveled in 5-minute time-bins over a 210-minute period after the administration of **(D)** tranylcypromine (10 mg/kg) and **(E)** a combination of clorgiline and rasagiline (10 and 3 mg/kg, respectively). The intraperitoneal injection was administered at time 0 of the graphs. **(F)** Representative path tracings of **(D)** and **(E)** obtained from 120th to 140th minute of recording. **(G)** Bar graphs showing the total distance traveled from the 90th to the 210th minute of recording. WT vs. TAAR1-KO, *$p < .01$; saline vs. drug, #$p < .01$, Tukey's honestly significant difference. Data are expressed as mean ± SEM. The number of the samples for each group is indicated on each of the bars. C, clorgiline; KO, knockout; ns, nonsignificant; R, rasagiline; S, saline; T, tranylcypromine; WT, wild-type.

values unveiled that the first component significantly separated the TCP-treated striata of the two genotypes in both intact and lesioned states (Figure 2E, Figure S6, and Table S6). In contrast, we did not observe any significant separation in the saline counterparts (Figure 2E, Figure S6, and Table S6). The second component significantly divided the samples according to the 6-OHDA lesion factor in both genotypes and treatments (Figure 2E, Figure S5, and Table S6). With the aim of showing the strength of each metabolite to influence each component of the t-score plot (Figure 2E), we performed a

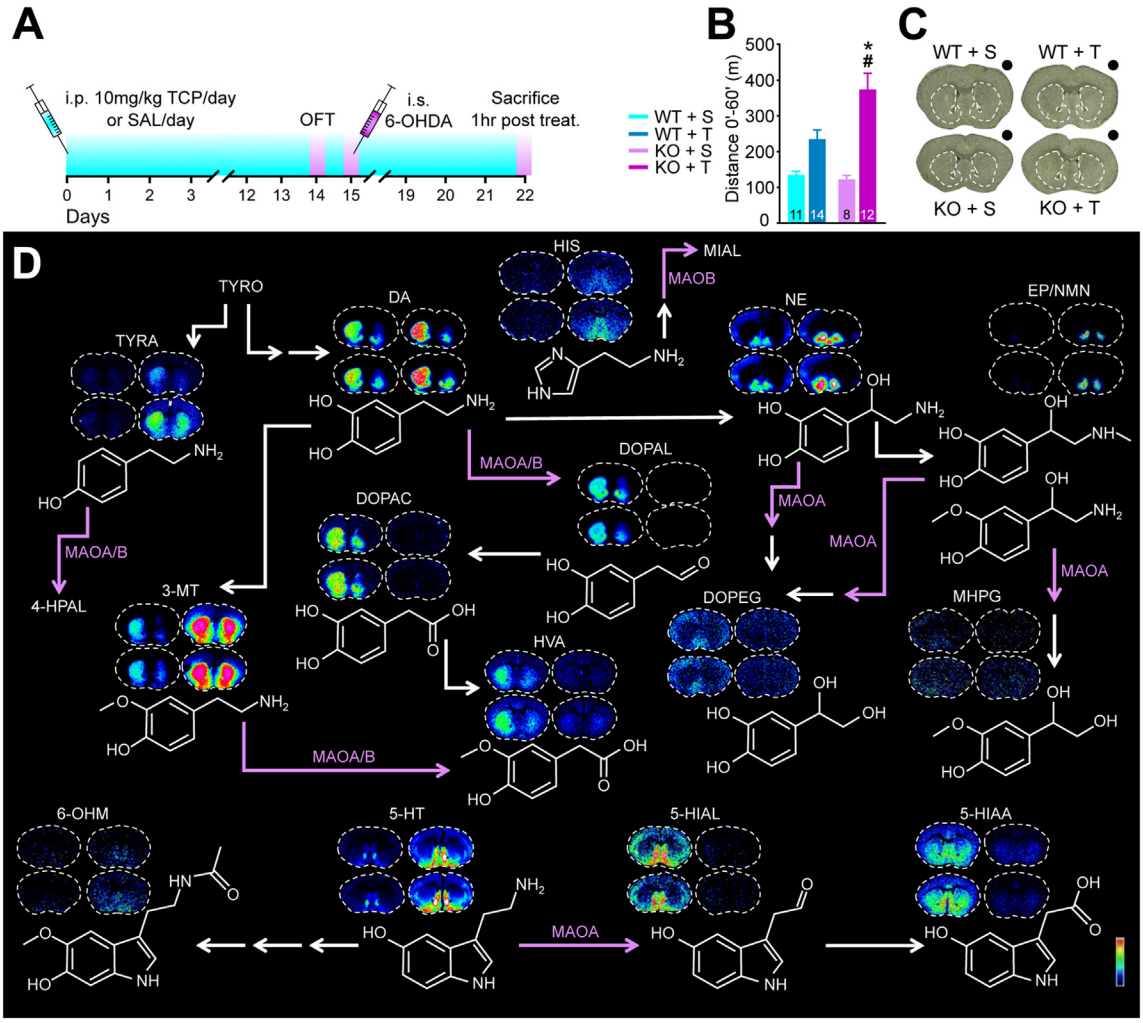
A
i.p. 10mg/kg TCP/day or SAL/day
OFT
i.s. 6-OHDA
Sacrifice 1hr post treat.
Days
B
Distance 0'-60' (m)
WT + S
WT + T
KO + S
KO + T
C
WT + S
WT + T
KO + S
KO + T
D
TYRO
TYRA
DA
HIS
MIAL
MAOB
NE
EP/NMN
MAOA/B
DOPAL
DOPAC
MAOA
4-HPAL
3-MT
DOPEG
MHPG
HVA
6-OHM
5-HT
5-HIAL
5-HIAA

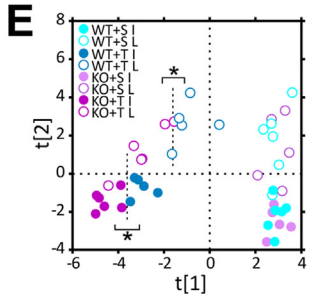
E
t[1]
t[2]

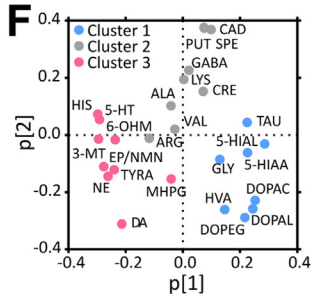
F
Cluster 1
Cluster 2
Cluster 3
p[1]
p[2]

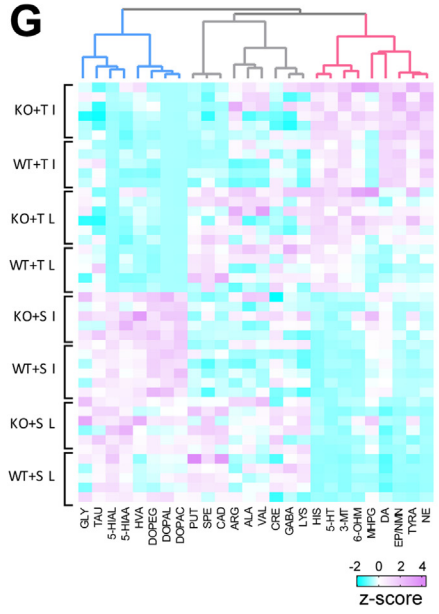
G
z-score

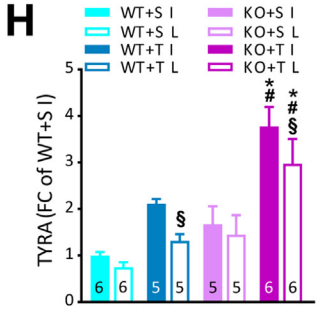
H
TYRA (FC of WT+S I)

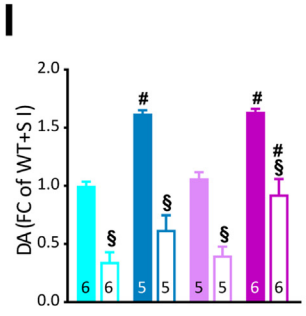
I
DA (FC of WT+S I)

loading plot of each peak (Figure 2F). The metabolites positioned before and after the MAO degradation step were robustly represented in the opposite limits along with the first component, while diamines were substantially characterized by the second component (Figure 2F). At the same time, amino acids and non-monoamine-related compounds were not well represented (Figure 2F). With the intention to categorize these different groups of metabolites, we performed hierarchical clustering and identified three different clusters (Figure 2G). Looking carefully at the different identified peaks, tyramine showed robust treatment and genotype-related changes (Figure 2H). We confirmed the authenticity of the tyramine peak by using tandem MSI (Figure S6). Three-way RM ANOVA showed that the tyramine peak was significantly affected by both genotype and treatment factors (Figure 2H and Table S2). Post hoc test revealed that tyramine was significantly higher in both hemispheres from TCP-treated TAAR1-KO mice than WT mice (Figure 2H). However, tyramine was significantly affected by the lesion (Figure 2H and Table S7), indicating that the metabolite is mainly derived by DA terminals. In contrast to the highly significant differences in tyramine between WT and TAAR1-KO animals, we did not observe any significant differences regarding the major monoamine neurotransmitters (DA, 5-HT, and NE) and diamines (Figure 2I, Figures S4 and S7, and Tables S7–S9). However, we identified that TAAR1-KO mice exhibited altered levels of histamine, 6-hydroxymelatonin, and taurine after TCP administration when compared with their WT counterparts (Figures S4 and S7 and Tables S8 and S9). In summary, TCP strongly increased tyramine levels in both intact and lesioned hemispheres. The stimulatory effect of TCP on tyramine levels was further enhanced in TAAR1-KO mice.

TCP Cause Enhanced Striatonigral *Arc* Gene Expression, Particularly in TAAR1-KO Mice

Both psychostimulants and antidepressants can increase striatal immediate early genes' messenger RNA levels (44,45). We examined striatal *Arc* after TCP administration to the unilaterally 6-OHDA lesioned mice (Figure 2A). Three-way RM ANOVA showed a significant upregulation of striatal *Arc* by TCP, which was more prominent in TAAR1-KO mice than WT mice (Figure 3A and Table S10). WT mice displayed significant *Arc* upregulation, which was significantly lower in the 6-OHDA lesioned side (Figure 3A and Table S10). There are two main subtypes of striatal projection neurons, D1 medium spiny neurons, which express *Pdyn*, and D2 medium spiny neurons, which express *Penk*. There was significant upregulation of striatal *Pdyn* messenger RNA with TCP treatment (Figure 3B and Table S10). Post hoc test revealed that *Pdyn* was significantly upregulated in TAAR1-KO mice but not in WT mice (Figure 3B). Regarding *Penk* and *Ppp1r1b*, there was no significant effect of treatment, genotype, or 6-OHDA (Figure S8 and Table S11). Because of the significant drug effect on *Pdyn* in TAAR1-KO mice, we performed double fluorescence in situ hybridization (RNAscope) in the intact striatum by combining *Arc* and *Pdyn* probes (Figure 3C, D). We found a significant increase of double-positive *Arc*/*Pdyn* neurons in both genotypes, which was more prominent in the TAAR1-KO mice (Figure 3E, F and Table S10). There was no significant change in the number of *Arc*-positive/*Pdyn*-negative cells in both genotypes (Figure 3F). To unveil a possible role of tyramine in activating striatonigral neurons, we used a supervised dimensionality reduction method. For this reason, we performed partial least squares analysis including both the MALDI and *Arc* data of the TCP-treated mice (Figure 3G). We first performed the loading plot to show which metabolite(s) were mostly related to *Arc* changes (Figure 3G and Table S12). Through the correlation matrix, we observed that *Arc* levels in both intact and lesioned striata show the highest correlation with tyramine change (Figure 3H and Table S13). Taken together, the observed increase of *Arc* on TCP treatment appears to be largely attributed to increased striatal tyramine content, particularly in TAAR1-KO mice.

MAO Inhibition Regulates Presynaptic Glutamate Release on DA Neurons Through TAAR1

The TAAR1-KO mouse line has a β-galactosidase reporter (29). We decided to use X-gal staining to identify the cells that exhibit an active TAAR1 promoter combined with immunofluorescent techniques. To validate the specificity of β-galactosidase for TAAR1, we used murine pancreatic tissue and observed an enrichment of X-gal precipitates in pancreatic islets (46,47) (Figure S9). We next confirmed that TAAR1 is

Figure 2. TCP increases tyramine particularly in TAAR1-KO mice. **(A)** Schematic depiction of the chronic TCP treatment timeline. **(B)** Bar graphs showing the total distance traveled from the 1st to the 60th minute of recording. WT vs. TAAR1-KO, $*p < .05$; S vs. T, $\#p < .001$, Tukey's honestly significant difference. **(C)** Representative pictures showing the striatal area used for quantification and the distribution of the three primary monoamine neurotransmitters and metabolites among the different groups. The lesioned side is located on the right-hand side of each image (black circle). **(D)** Representative images for each peak among the different groups (left upper: WT+S group; right upper: WT+T group; left lower: TAAR1-KO+S; right lower: TAAR1-KO+T). Each peak is accompanied by its chemical structure. The arrows denote the metabolic pathways between each metabolite. The magenta arrows denote a MAO-dependent chemical reaction. **(E)** Scores plot of the first (t[1]) and second (t[2]) principal components, based on the 95% confidence interval hoteling ellipse, derived from principal component analysis with all samples (WT/TAAR1-KO, S/T, I/L) and measured metabolites being included. Significant differences according to t[1] values are indicated; WT vs. TAAR1-KO: $*p < .01$, Tukey's honestly significant difference. Objects are colored according to different groups. **(F)** Corresponding loadings plot (p[1] vs. p[2]) showing how the variables (i.e., metabolites) correlate with each other and contribute to the model. Variables are colored according to grouping performed by hierarchical clustering analysis. **(G)** *z* Score matrix of the FCs of the metabolites (columns) in each individual (rows). Shown above the matrix is the hierarchical clustering dendrogram. **(H, I)** Bar graph showing the quantification of the **(H)** tyramine and **(I)** DA peaks. WT vs. TAAR1-KO, $*p < .05$; S vs. T, $\#p < .01$; I vs. L, $\S p < .001$, Tukey's honestly significant difference. The number of samples for each group is indicated on each of the bars. 3-MT, 3-methoxytyramine; 4-HPAL, 4-hydroxyphenylacetaldehyde; 5-HIAA, 5-hydroxyindoleacetic acid; 5-HIAL, 5-hydroxyindoleacetaldehyde; 5-HT, serotonin; 6-OHDA, 6-hydroxydopamine; 6-OHM, 6-hydroxymelatonin; ALA, alanine; ARG, arginine; CAD, cadaverine; CRE, creatinine; DA, dopamine; DOPAC, dihydroxyphenylacetic acid; DOPAL, dihydroxyphenylacetaldehyde; DOPEG, dihydroxyphenylethylene glycol; EP/NMN, epinephrine/normetanephrine; FC, fold change; GABA, gamma-aminobutyric acid; GLY, glycine; HIS, histamine; HVA, homovanillic acid; I, intact; i.s., intrastriatal; KO, knockout; L, lesion; LYS, lysine; MAO, monoamine oxidase; MHPG, methoxyhydroxyphenylglycol; NE, norepinephrine; OFT, open field test; PUT, putrescine; S, saline; SAL, saline; SPE, spermidine; T, tranylcypromine; TAU, taurine; TCP, tranylcypromine; TYRA, tyramine; VAL, valine; WT, wild-type.

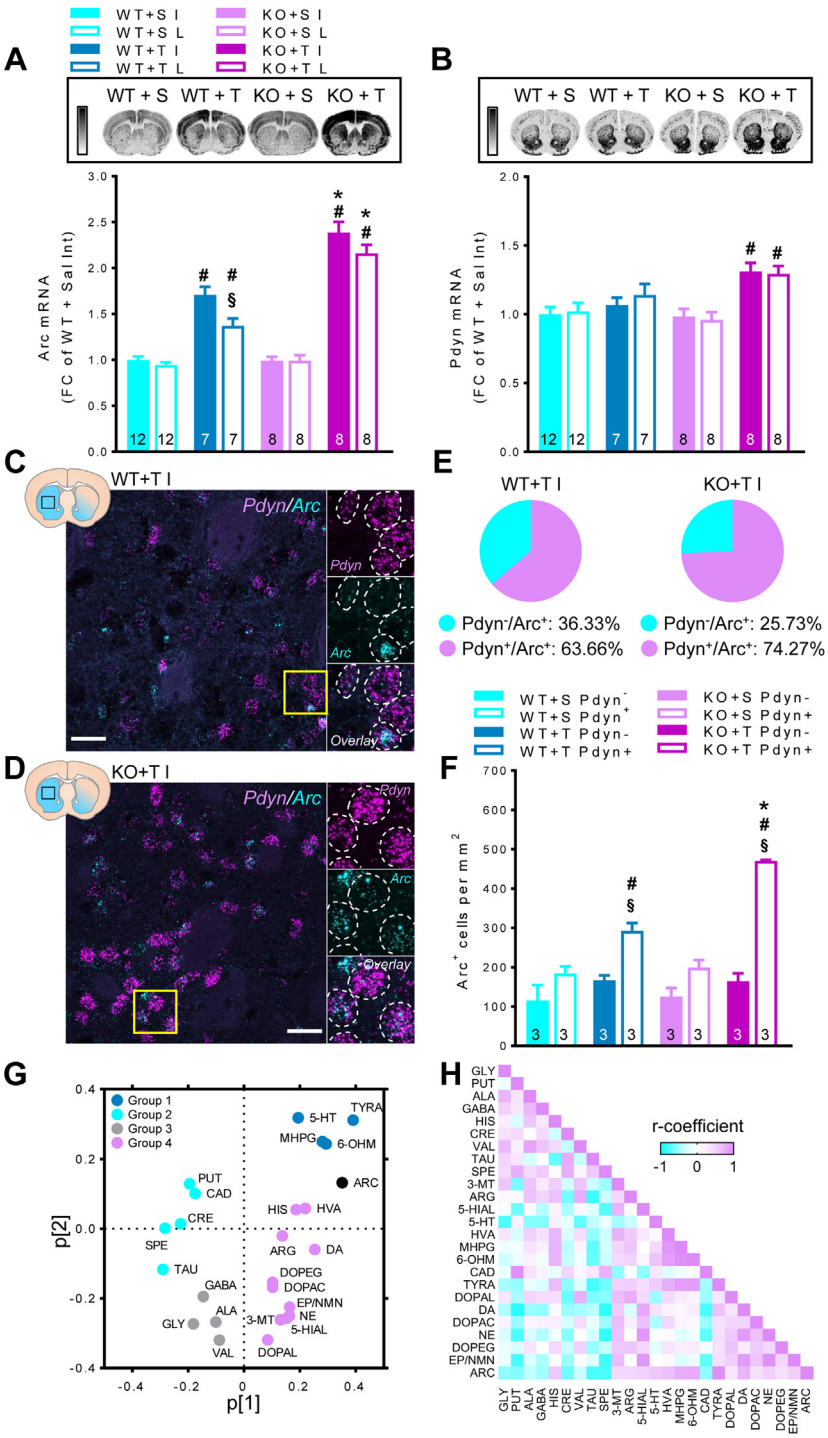

Figure 3. TAAR1-KO display enhanced monoamine oxidase inhibitor–induced gene upregulation in striatum, which are correlated with tyramine. **(A, B)** Bar graphs showing the striatal mRNA levels of **(A)** *Arc* and **(B)** *Pdyn*, quantified by radioactive in situ hybridization. $n = 3$; WT vs. TAAR1-KO, $^{*}p < .001$; S vs. T, $\#p < .05$; I vs. L, $\S p < .01$, Tukey's honestly significant difference. **(C, D)** Representative images of RNAscope in the intact striata of **(C)** WT and **(D)** TAAR1-KO–treated animals showing the increase in number of $Pdyn^{+}/Arc^{+}$ cells. Scale bars = 30 μm. **(E)** Pie charts showing the percentage of $Pdyn^{+}/Arc^{+}$ cells increased in TAAR1-KO–treated animals compared with the WT animals. **(F)** Bar graphs depicting the increased number of $Pdyn^{+}/Arc^{+}$ cells in TAAR1-KO tranylcypromine-treated striata. $n = 3$, WT vs. TAAR1-KO, $^{*}p < .01$; S vs. T, $\#p < .05$; $Pdyn^{+}$ vs. $Pdyn^{-}$, $\S p < .01$, Tukey's honestly significant difference. **(G)** Loadings plot of p[1] and p[2], derived from partial least squares analysis of mRNA FC data, for tranylcypromine-treated I/L samples. Variables are colored according to grouping performed by hierarchical clustering analysis. **(H)** Corresponding correlation matrix based on Pearson's correlation coefficient for all metabolites included in the partial least squares model. Data are expressed as mean ± SEM. The number of the samples for each group is indicated on each of the bars. 3-MT, 3-methoxytyramine; 5-HIAL, 5-hydroxyindoleacetaldehyde; 5-HT, serotonin; 6-OHM, 6-hydroxymelatonin; ALA, alanine; ARG, arginine; CAD, cadaverine; CRE, creatinine; DA, dopamine; DOPAC, dihydroxyphenylacetic acid; DOPAL, dihydroxyphenylacetaldehyde; DOPEG, dihydroxyphenylethylene glycol; EP/NMN, epinephrine/normetanephrine; FC, fold change; GABA, gamma-aminobutyric acid; GLY, glycine; HIS, histamine; HVA, homovanillic acid; I, intact; KO, knockout; L, lesion; MHPG, methoxyhydroxyphenylglycol; mRNA, messenger RNA; NE, norepinephrine; p[1], first principal component; p[2], second principal component; PUT, putrescine; S, saline; SPE, spermidine; T, tranylcypromine; TAU, taurine; TYRA, tyramine; VAL, valine; WT, wild-type.

located in tyrosine hydroxylase (TH) neurons of both SNc and VTA (Figure 4A, B). In addition, we described for the first time that TAAR1 is expressed in non-DA cells such as the medial bed nucleus of the stria terminalis (BSTM), lateral hypothalamic area, zona incerta, and dorsolateral parabrachial nucleus (LPBD) (Figure 4A, B). These regions send strong projections to DA neurons of SNc and VTA (48–54). Consequently, we hypothesized that TAAR1 may regulate the presynaptic glutamatergic drive of DA cells and performed FAST recordings in SNc after the local application of TCP, tyramine, and EPPTB in

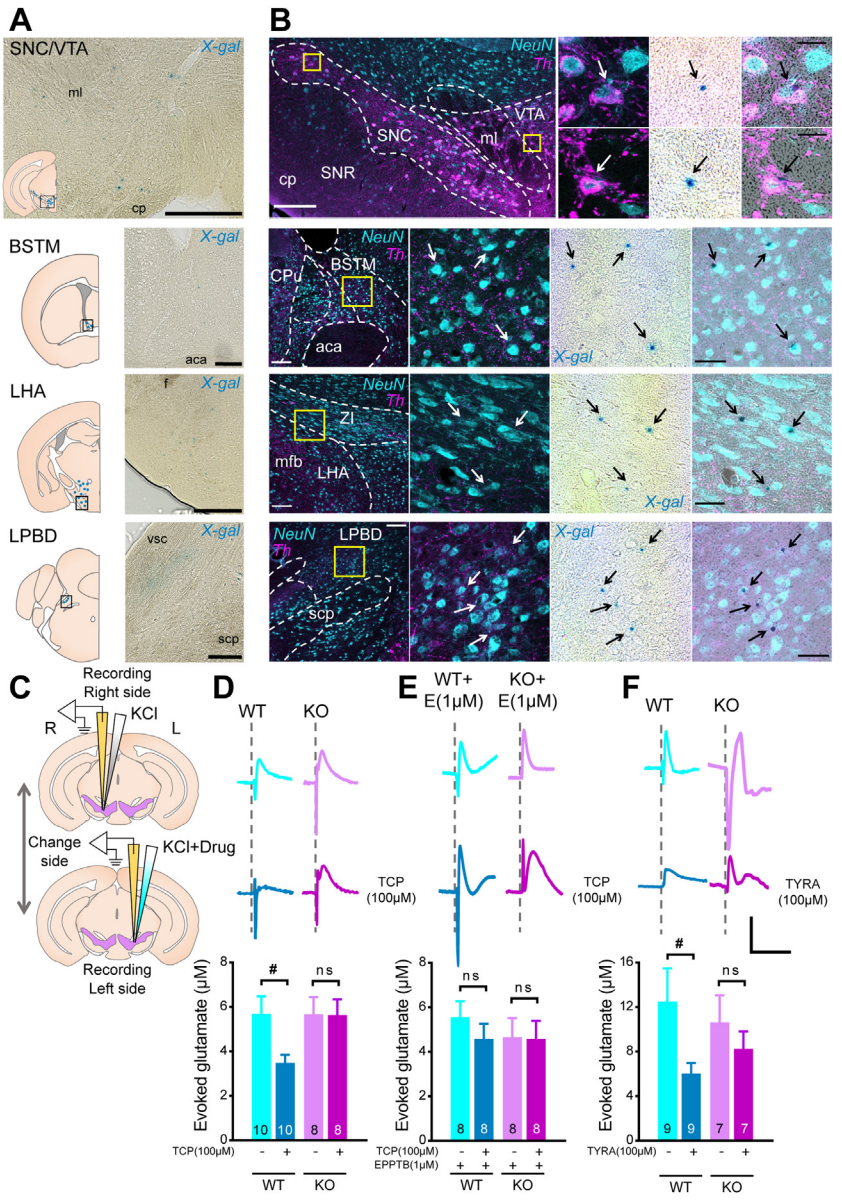

Figure 4. TAAR1 is expressed outside of dopamine neurons and regulates glutamate release in the ventral midbrain. **(A)** Histoenzymological detection of TAAR1 with X-gal staining in SNC/VTA, BSTM, ZI/LHA, and LPBD. SNC/VTA scale bar = 250 μm, BSTM scale bar = 100 μm, ZI/LHA scale bar = 250 μm, LPBD scale bar = 100 μm. **(B)** Combined X-gal and immunofluorescence stainings, showing the expression of TAAR1 in SNC/VTA, BSTM, ZI/LHA, and LPBD. Regarding the immunofluorescence pictures, cyan represents NeuN (neuronal marker) and magenta depicts Th. Notably, triple X-gal$^+$/Th$^+$/NeuN$^+$ cells are found in SNC/VTA, while in BSTM, ZI/LHA, and LPBD, there are only X-gal$^+$/NeuN$^+$/Th$^-$. SNC/VTA: left scale bar = 100 μm, right scale bar = 10 μm; BSTM, ZI/LHA, and LPBD: left scale bar = 100 μm, right scale bar = 20 μm. **(C)** Schematic depiction of the experimental procedure of FAST in anesthetized animals. First, KCl (vehicle) recordings were carried out on the right hemisphere. Afterward, the electrode was placed to the left hemisphere where the recordings combined with local drug application took place. **(D–F)** Bar graph with representative traces of the recordings showing the evoked glutamate release (in μM) after the local application of **(D)** TCP, **(E)** TCP/EPPTB, and **(F)** tyramine. Saline vs. TCP, #$p < .05$, Tukey's honestly significant difference. Vertical scale bar = 1 μM, horizontal scale bar = 20 ms. Data are expressed as mean ± SEM. The number of the samples for each group is indicated on each of the bars. aca, anterior part of anterior commissure; BSTM, medial bed nucleus of the stria terminalis; cp, cerebral peduncle; CPu, caudoputamen; E, EPPTB; f, fornix; FAST, fast analytical sensing technology; KCl, potassium chloride; KO, knockout; LPBD, dorsolateral parabrachial nucleus; LHA, lateral hypothalamic area; mfb, medial forebrain bundle; ml, medial lemniscus; ns, nonsignificant; scp, superior cerebellar peduncle; SNC, substantia nigra pars compacta; SNR, substantia nigra pars reticulata; TCP, tranylcypromine; Th, tyrosine hydroxylase; TYRA, tyramine; vsc, ventral spinocerebellar tract; VTA, ventral tegmental area; WT, wild-type; ZI, zona incerta.

WT and TAAR1-KO mice (Figure 4C). Two-way RM ANOVA on FAST data showed a significant effect of TCP (100 μM) application and interaction of genotype with drug factor (Figure 4D and Table S14). Post hoc analysis showed significant downregulation of glutamate release by TCP in WT but not in TAAR1-KO mice. Two-way RM ANOVA showed that the co-application of the TAAR1 antagonist EPPTB abolishes the effect of TCP in WT mice (Figure 4E and Table S14). Subsequently, we performed FAST recordings with local tyramine (100 μM) application. Tyramine significantly reduced glutamate release in WT but not in TAAR1-KO mice (Figure 4F and Table S14). To investigate whether TAAR1 blocks glutamate release after stimulatory doses of TCP, we performed simultaneous ventral midbrain glutamate recordings and open field activity after acute systemic administration of 10 mg/kg TCP in freely moving mice (Figure 5A–D). Two-way RM ANOVA showed a significant interaction of genotype and treatment factor in 90 and 140 minutes in both open field activity and glutamate release (Figure 5E–I and Tables S15 and S16). Post hoc test showed a significant increase in both glutamate release and locomotor activity after TCP in TAAR1-KO mice but not in WT mice (Figure 5E–I). In summary, in addition to the direct action of tyramine/TAAR1 on DA neurons (27), we provide evidence that TAAR1 participates in a tyramine-mediated negative feedback mechanism of glutamatergic facilitation in DA neurons after MAO inhibition.

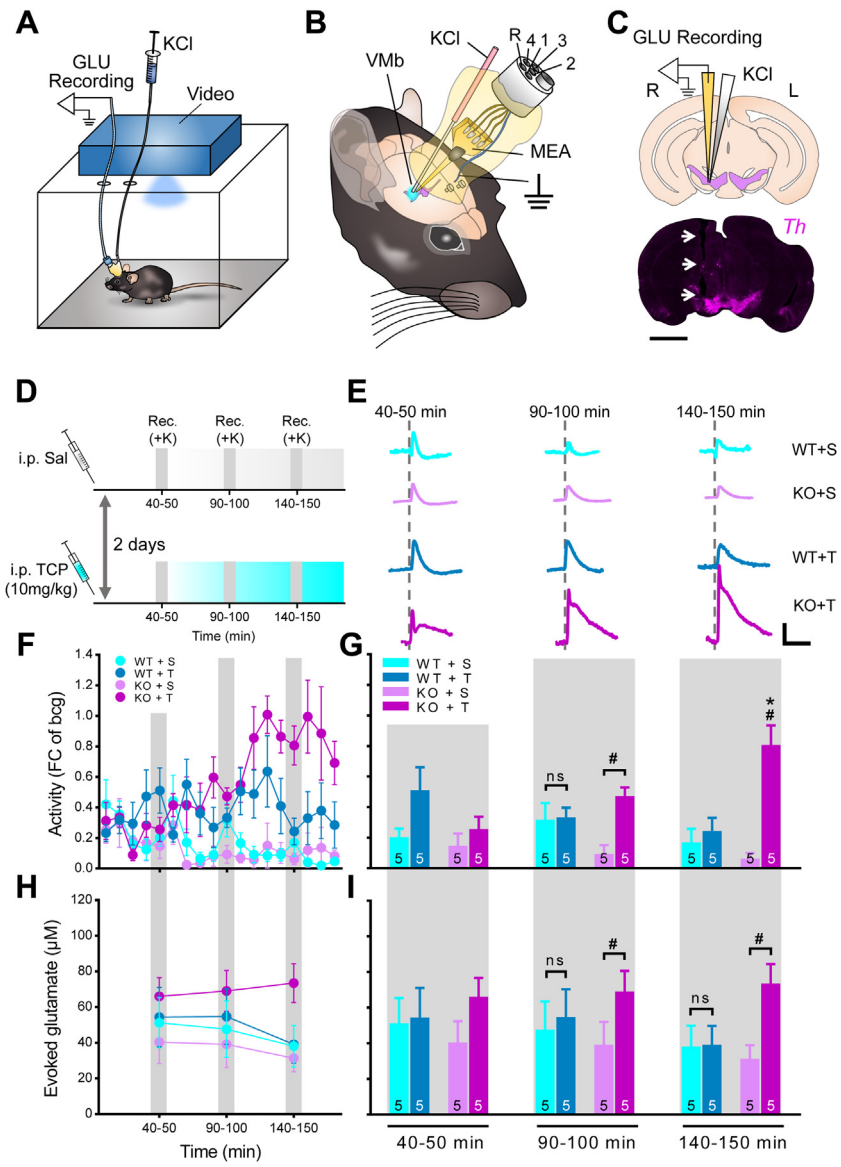

Figure 5. TAAR1 blocks glutamate release facilitation in ventral midbrain after monoamine oxidase inhibition in freely moving mice. **(A, B)** Schematic representation of the experimental setup in the freely moving FAST recordings. **(C)** Validation of the MEA positioning within the Th^+ (magenta) area of ventral midbrain. The track of the MEA is shown with white arrows (scale bar = 1 mm). **(D)** Schematic depiction of freely moving FAST recording time plan. **(E)** Representative recording traces of freely moving FAST for each time point and group. Vertical scale bar = 1 μM, horizontal scale bar = 20 ms. **(F)** Line graph showing the activity recordings in 10-minute time-bins over a 180-minute period. **(G)** Bar graph showing the 10-minute activity after the 40th, 90th, and 140th minute of S/TCP delivery. WT vs. TAAR1-KO, $*p < .05$; S vs. T, $\#p < .05$, Tukey's honestly significant difference. **(H)** Line graph showing the evoked glutamate release concentration (recording duration: 10 min) over the total experimental procedure. **(I)** Bar graph depicting the evoked glutamate release concentration after the 40th, 90th, and 140th minute of saline/TCP delivery: ns; S vs. T, $\#p < .05$, Tukey's honestly significant difference. Data are expressed as mean ± SEM. The number of the samples for each group is indicated on each of the bars. FAST, fast analytical sensing technology; FC, fold change; GLU, glutamate; i.p., intraperitoneal; KCl, potassium chloride; KO, knockout; MEA, microelectrode array; ns, nonsignificant; R, reference; Rec., recording; S, saline; Sal, saline; T, tranylcypromine; TCP, tranylcypromine; Th, tyrosine hydroxylase; VMb, ventral midbrain; WT, wild-type.

DISCUSSION

TAAR1 Prevents the Aberrant Accumulation of Tyramine Following MAOI Administration

The finding acquired using MSI that TCP strongly increases tyramine in the striatum of TAAR1-KO mice suggests that TAAR1 negatively regulates central tyramine levels in a feedback manner. The MSI data also showed that the tyramine signal is reduced by striatal 6-OHDA lesioning, indicating that the accumulation of tyramine may principally occur in DA neurons. Previous work has shown that striatal tyramine levels are directly determined by TH enzymatic activity (55). Reduced TH-mediated conversion of tyrosine to dihydroxyphenylalanine leads to a secondary increase in decarboxylation to tyramine through AADC. We propose that TAAR1 is strategically positioned intracellularly to sense increases in tyramine concentration and suppress the further and potentially disruptive accumulation of this TA. Further supporting this hypothesis, we have previously found that TAAR1 increases TH activity through phosphorylation of serines 19 and 40 (16). In the literature, a heightened firing rate of DA neurons in TAAR1-KO mice is reported (24,26–28), which is consistent with the accumulation of tyramine on MAO inhibition found in this study. DA neuronal activity is negatively regulated by dopamine D_2 autoreceptors (56–58). Accordingly, a TAAR1-D_2 autoreceptor heteromeric complex may enhance D_2-mediated autoinhibition so as to alleviate the tyramine overload (59,60).

TCP-Induced Tyramine, *Arc*, and Locomotor Responses Are Increased in TAAR1-KO Mice

The observed excess of striatal tyramine in TAAR1-KO mice correlated with increased *Arc* in striatonigral neurons. Though messenger RNA is a poor predictor of levels of the protein itself, it has been repeatedly shown that activation of *Arc* is related to an increase in synaptic activity (61–64). Upregulation of *Arc* is found after cocaine or amphetamine treatment (65–67), and heightened striatonigral cell activity contributes to the increased locomotor response (68). Tyramine has amphetamine-like properties, and its DA-releasing actions may be amplified in the striatum of TAAR1-KO mice (11). Moreover, additional mechanisms, such as MAOI-mediated elevations of DA in the striatum and SNc, may also contribute to increased *Arc* and locomotion.

TAAR1 Counteracts the Glutamate Release in SNc After MAOI Treatment

TAAR1 suppresses neuronal activity and the frequency of excitatory postsynaptic currents in DA neurons, indicating a role for TAAR1-mediated actions on glutamate afferents (28). However, TAAR1 has been reported to have no or only low expression in glutamatergic neurons of the subthalamic nucleus, prefrontal cortex, and pedunculopontine nucleus (24,29), which innervate DA neurons (69). We reveal here that TAAR1 is expressed in nondopaminergic neurons of BSTM, lateral hypothalamic area/zona incerta, and LPBD, which also send glutamatergic projections to SNc/VTA DA neurons (49–54). It has been shown that BSTM controls the cocaine-induced locomotor response through activation of VTA DA neurons (54). Moreover, optogenetic stimulation of glutamatergic neurons in LPBD projecting to SNc induces striatal DA release in mice (49). Consequently, TAAR1 might regulate the excitability of these areas and accordingly ameliorate the TCP-induced locomotor response. By using an enzyme-based biosensor technology, we found that TCP and tyramine reduced glutamate release in SNc in WT but not in TAAR1-KO mice. Our data indicate that TAAR1 located in BSTM, lateral hypothalamic area/zona incerta, and LPBD is activated by tyramine and reduces glutamate release from these regions in the ventral midbrain. Albeit, inasmuch as both TCP and tyramine show similar effects on glutamate release, TCP's effect might also involve other mechanisms such as elevation of DA, which exhibits weak agonist properties to TAAR1 (20,70,71).

It is also possible that the influence of tyramine and TCP on glutamate levels involves the recently reported TAAR1-mediated regulation of trafficking of EAAT3 in DA cells (17). It is also noteworthy that EAAT1 and EAAT2, along with TAAR1, are expressed in astrocytes (72–74). Although the data from both local administration of TCP in anesthetized mice and systemic administration in freely moving animals indicate a suppressive role of TAAR1 on glutamate levels, the nature of the responses differs. These differences might originate from the fact that systemic TCP administration stimulates multiple monoaminergic systems and circuitries that cannot be activated by local drug application. As a result, systemic TCP may cause a generalized hyperactivity of glutamatergic SNc afferents that is normalized by an action of TAAR1. Another obvious aspect of the differences between anesthetized and freely moving animals is the alertness. In agreement with our data, it has been shown that isoflurane reduces glutamate release (75).

TAAR1 Limits the Changes of Several Amines but Not Diamines

In addition to tyramine, we identified alterations in the levels of histamine, the melatonin metabolite 6-hydroxymelatonin, and taurine after TCP. Histamine and 6-hydroxymelatonin displayed an enhanced accumulation in TAAR1-KO versus WT mice, while taurine showed an opposite trend after TCP treatment. Histamine, melatonin, and taurine are well-known amines associated with sleep induction (76–79). Both genetic and pharmacological manipulation of TAAR1 alters wakefulness and sleep states (80,81). Even though our data are restricted to the caudoputamen and nucleus accumbens, there is evidence that striatal areas are involved in sleep-wake cycle regulation (82). We also observed that 6-OHDA injection caused a significant increase of diamines such as cadaverine, putrescine, and spermidine. Although TAAR1 does not affect the accumulation of these TAs, other TAARs expressed in periventricular zones might be involved in this effect (22,83).

Conclusions

Using the clinically applied antidepressant MAOI TCP as a tool to elevate central levels of tyramine, our data suggest an important role for tyramine in behavioral, transcriptional, and neurochemical actions of MAO inhibition. These effects of tyramine are enhanced in TAAR1-KO mice via several TAAR1-independent and TAAR1-dependent mechanisms, which warrants further exploration. Our data strongly indicate that tyramine is not only mediating side effects of MAOIs but may play a critical role in therapeutic responses of these commonly used pharmaceutical agents.

ACKNOWLEDGMENTS AND DISCLOSURES

This study was supported by Konung Gustaf V:s och Drottning Victorias Frimurarestiftelse (Grant No. 2019 [to PS]) and the Swedish Research Council (Grant No. 2019-01422 [to PS]); the Swedish Research Council (Medicine and Health; Grant No. 2018-03320 [to PEA]), Natural and Engineering Science (Grant No. 2018-05501 [to PEA]), the Swedish Brain Foundation (Grant No. FO2018-0292 [to PEA]), Marie Skłodowska-Curie Actions, Uppsala University (Research Infrastructure), the Swedish Foundation for Strategic Research (Grant No. RIF14-0078 [to PEA]), and Science for Life Laboratory (SciLifeLab) (to PEA); and the Karolinska Institutet National Institutes of Health program and the Swedish Medical Association (to XZ and IM).

MJM is a full-time employee of Servier Research Institute. All other authors report no biomedical financial interests or potential conflicts of interest.

ARTICLE INFORMATION

From the Department of Neurology and Clinical Neuroscience (IM, YY, MK, XZ, PS), Karolinska Institutet, Stockholm; Department of Pharmaceutical Biosciences (TV, MS, EF, PEA), Medical Mass Spectrometry Imaging, Uppsala University; and National Resource for Mass Spectrometry Imaging (MS, PEA), Science for Life Laboratory, Uppsala University, Uppsala, Sweden; and the Centre for Therapeutic Innovation-CNS (MJM), Institut de Recherches Servier, Centre de Recherches de Croissy, Paris, France.

Address correspondence to Ioannis Mantas, M.D., at ioannis.mantas@ki.se.

Received Oct 12, 2020; revised Dec 7, 2020; accepted Dec 11, 2020.

Supplementary material cited in this article is available online at https://doi.org/10.1016/j.biopsych.2020.12.008.

REFERENCES

1. Berton O, Nestler EJ (2006): New approaches to antidepressant drug discovery: Beyond monoamines. Nat Rev Neurosci 7:137–151.
2. Youdim MBH, Edmondson D, Tipton KF (2006): The therapeutic potential of monoamine oxidase inhibitors. Nat Rev Neurosci 7:295–309.
3. Schildkraut JJ, Herzog JM, Orsulak PJ, Edelman SE, Shein HM, Frazier SH (1976): Reduced platelet monoamine oxidase activity in a subgroup of schizophrenic patients. Am J Psychiatry 133:438–440.
4. Wyatt RJ, Murphy DL, Belmaker R, Cohen S, Donnelly CH, Pollin W (1973): Reduced monoamine oxidase activity in platelets: A possible genetic marker for vulnerability to schizophrenia. Science 179:916–918.
5. Jacob CP, Müller J, Schmidt M, Hohenberger K, Gutknecht L, Reif A, *et al.* (2005): Cluster B personality disorders are associated with allelic variation of monoamine oxidase A activity. Neuropsychopharmacology 30:1711–1718.
6. Zucchi R, Chiellini G, Scanlan TS, Grandy DK (2006): Trace amine-associated receptors and their ligands. Br J Pharmacol 149:967–978.
7. Gainetdinov RR, Hoener MC, Berry MD (2018): Trace amines and their receptors. Pharmacol Rev 70:549–620.
8. Sandler M, Ruthven CR, Goodwin BL, Reynolds GP, Rao VA, Coppen A (1979): Deficient production of tyramine and octopamine in cases of depression. Nature 278:357–358.
9. D'Andrea G, Pizzolato G, Gucciardi A, Stocchero M, Giordano G, Baraldi E, Leon A (2019): Different circulating trace amine profiles in de novo and treated Parkinson's disease patients. Sci Rep 9:6151.
10. Von Voigtlander PF, Moore KE (1973): Involvement of nigro-striatal neurons in the in vivo release of dopamine by amphetamine, amantadine and tyramine. J Pharmacol Exp Ther 184:542–552.
11. Sulzer D, Rayport S (1990): Amphetamine and other psychostimulants reduce pH gradients in midbrain dopaminergic neurons and chromaffin granules: A mechanism of action. Neuron 5:797–808.
12. Juorio AV (1979): Drug-induced changes in the formation, storage and metabolism of tyramine in the mouse. Br J Pharmacol 66:377–384.
13. Blackwell B, Mabbitt LA (1965): Tyramine in cheese related to hypertensive crises after monoamine-oxidase inhibition. Lancet 1:938–940.
14. Khan MZ, Nawaz W (2016): The emerging roles of human trace amines and human trace amine-associated receptors (hTAARs) in central nervous system. Biomed Pharmacother 83:439–449.
15. Rutigliano G, Accorroni A, Zucchi R (2018): The case for TAAR1 as a modulator of central nervous system function. Front Pharmacol 8:987.
16. Zhang X, Mantas I, Alvarsson A, Yoshitake T, Shariatgorji M, Pereira M, *et al.* (2018): Striatal tyrosine hydroxylase is stimulated via TAAR1 by 3-iodothyronamine, but not by tyramine or β-phenylethylamine. Front Pharmacol 9:166.
17. Underhill SM, Hullihen PD, Chen J, Fenollar-Ferrer C, Rizzo MA, Ingram SL, Amara SG (2019): Amphetamines signal through intracellular TAAR1 receptors coupled to $G\alpha_{13}$ and $G\alpha_{S}$ in discrete subcellular domains [published online ahead of print Aug 9]. Mol Psychiatry.
18. Xie Z, Miller GM (2007): Trace amine-associated receptor 1 is a modulator of the dopamine transporter. J Pharmacol Exp Ther 321:128–136.
19. Michael ES, Covic L, Kuliopulos A (2019): Trace amine-associated receptor 1 (TAAR1) promotes anti-diabetic signaling in insulin-secreting cells. J Biol Chem 294:4401–4411.
20. Bunzow JR, Sonders MS, Arttamangkul S, Harrison LM, Zhang G, Quigley DI, *et al.* (2001): Amphetamine, 3,4-methylenedioxymethamphetamine, lysergic acid diethylamide, and metabolites of the catecholamine neurotransmitters are agonists of a rat trace amine receptor. Mol Pharmacol 60:1181–1188.
21. Espinoza S, Sukhanov I, Efimova EV, Kozlova A, Antonova KA, Illiano P, *et al.* (2020): Trace amine-associated receptor 5 provides olfactory input into limbic brain areas and modulates emotional behaviors and serotonin transmission. Front Mol Neurosci 13:18.
22. Efimova EV, Kozlova AA, Razenkova V, Katolikova NV, Antonova KA, Sotnikova TD, *et al.* (2021): Increased dopamine transmission and adult neurogenesis in trace amine-associated receptor 5 (TAAR5) knockout mice. Neuropharmacology 182:108373.
23. Liberles SD (2015): Trace amine-associated receptors: Ligands, neural circuits, and behaviors. Curr Opin Neurobiol 34:1–7.
24. Lindemann L, Meyer CA, Jeanneau K, Bradaia A, Ozmen L, Bluethmann H, *et al.* (2008): Trace amine-associated receptor 1 modulates dopaminergic activity. J Pharmacol Exp Ther 324:948–956.
25. Espinoza S, Lignani G, Caffino L, Maggi S, Sukhanov I, Leo D, *et al.* (2015): TAAR1 modulates cortical glutamate NMDA receptor function. Neuropsychopharmacology 40:2217–2227.
26. Bradaia A, Trube G, Stalder H, Norcross RD, Ozmen L, Wettstein JG, *et al.* (2009): The selective antagonist EPPTB reveals TAAR1-mediated regulatory mechanisms in dopaminergic neurons of the mesolimbic system. Proc Natl Acad Sci U S A 106:20081–20086.
27. Revel FG, Moreau JL, Gainetdinov RR, Bradaia A, Sotnikova TD, Mory R, *et al.* (2011): TAAR1 activation modulates monoaminergic neurotransmission, preventing hyperdopaminergic and hypoglutamatergic activity. Proc Natl Acad Sci U S A 108:8485–8490.
28. Revel FG, Meyer CA, Bradaia A, Jeanneau K, Calcagno E, André CB, *et al.* (2012): Brain-specific overexpression of trace amine-associated receptor 1 alters monoaminergic neurotransmission and decreases sensitivity to amphetamine. Neuropsychopharmacology 37:2580–2592.
29. Di Cara B, Maggio R, Aloisi G, Rivet JM, Lundius EG, Yoshitake T, *et al.* (2011): Genetic deletion of trace amine 1 receptors reveals their role in auto-inhibiting the actions of ecstasy (MDMA). J Neurosci 31:16928–16940.
30. Millan MJ (2006): Multi-target strategies for the improved treatment of depressive states: Conceptual foundations and neuronal substrates, drug discovery and therapeutic application. Pharmacol Ther 110:135–370.
31. Koblan KS, Kent J, Hopkins SC, Krystal JH, Cheng H, Goldman R, Loebel A (2020): A non-D2-receptor-binding drug for the treatment of schizophrenia. N Engl J Med 382:1497–1506.
32. Dedic N, Jones PG, Hopkins SC, Lew R, Shao L, Campbell JE, *et al.* (2019): SEP-363856, a novel psychotropic agent with a unique, non-D_2 receptor mechanism of action. J Pharmacol Exp Ther 371:1–14.
33. Shariatgorji M, Nilsson A, Fridjonsdottir E, Vallianatou T, Källback P, Katan L, *et al.* (2019): Comprehensive mapping of neurotransmitter networks by MALDI-MS imaging. Nat Methods 16:1021–1028.
34. Ulrich S, Ricken R, Adli M (2017): Tranylcypromine in mind (part I): Review of pharmacology. Eur Neuropsychopharmacol 27:697–713.
35. Ulrich S, Ricken R, Buspavanich P, Schlattmann P, Adli M (2020): Efficacy and adverse effects of tranylcypromine and tricyclic antidepressants in the treatment of depression: A systematic review and comprehensive meta-analysis. J Clin Psychopharmacol 40:63–74.
36. Mantas I, Yang Y, Mannoury-la-Cour C, Millan MJ, Zhang X, Svenningsson P (2020): Genetic deletion of GPR88 enhances the locomotor response to L-DOPA in experimental parkinsonism while counteracting the induction of dyskinesia. Neuropharmacology 162:107829.
37. Alvarsson A, Zhang X, Stan TL, Schintu N, Kadkhodaei B, Millan MJ, *et al.* (2015): Modulation by trace amine-associated receptor 1 of experimental parkinsonism, L-DOPA responsivity, and glutamatergic neurotransmission. J Neurosci 35:14057–14069.
38. Stan TL, Alvarsson A, Branzell N, Sousa VC, Svenningsson P (2014): NMDA receptor antagonists ketamine and Ro25-6981 inhibit evoked release of glutamate in vivo in the subiculum. Transl Psychiatry 4:e395.
39. Hascup KN, Hascup ER, Pomerleau F, Huettl P, Gerhardt GA (2008): Second-by-second measures of L-glutamate in the prefrontal cortex and striatum of freely moving mice. J Pharmacol Exp Ther 324:725–731.
40. Bourin M, Hascoët M, Colombel MC, Coutts RT, Baker GB (2002): Clonidine potentiates the effects of tranylcypromine, phenelzine and two analogues in the forced swimming test in mice. J Psychiatry Neurosci 27:178–185.
41. Guillem K, Vouillac C, Azar MR, Parsons LH, Koob GF, Cador M, Stinus L (2005): Monoamine oxidase inhibition dramatically increases the motivation to self-administer nicotine in rats. J Neurosci 25:8593–8600.
42. Villégier AS, Salomon L, Granon S, Changeux JP, Belluzzi JD, Leslie FM, Tassin JP (2006): Monoamine oxidase inhibitors allow locomotor and rewarding responses to nicotine. Neuropsychopharmacology 31:1704–1713.

43. Bajpai P, Sangar MC, Singh S, Tang W, Bansal S, Chowdhury G, *et al.* (2013): Metabolism of 1-methyl-4-phenyl-1,2,3,6-tetrahydropyridine by mitochondrion-targeted cytochrome P450 2D6: Implications in Parkinson disease. J Biol Chem 288:4436–4451.
44. Konradi C, Leveque JC, Hyman SE (1996): Amphetamine and dopamine-induced immediate early gene expression in striatal neurons depends on postsynaptic NMDA receptors and calcium. J Neurosci 16:4231–4239.
45. Slattery DA, Morrow JA, Hudson AL, Hill DR, Nutt DJ, Henry B (2005): Comparison of alterations in c-fos and Egr-1 (zif268) expression throughout the rat brain following acute administration of different classes of antidepressant compounds. Neuropsychopharmacology 30:1278–1287.
46. Raab S, Wang H, Uhles S, Cole N, Alvarez-Sanchez R, Künnecke B, *et al.* (2015): Incretin-like effects of small molecule trace amine-associated receptor 1 agonists. Mol Metab 5:47–56.
47. Revel FG, Moreau JL, Pouzet B, Mory R, Bradaia A, Buchy D, *et al.* (2013): A new perspective for schizophrenia: TAAR1 agonists reveal antipsychotic- and antidepressant-like activity, improve cognition and control body weight. Mol Psychiatry 18:543–556.
48. Juarez B, Han MH (2016): Diversity of dopaminergic neural circuits in response to drug exposure. Neuropsychopharmacology 41:2424–2446.
49. Han W, Tellez LA, Perkins MH, Perez IO, Qu T, Ferreira J, *et al.* (2018): A neural circuit for gut-induced reward [published correction appears in Cell 2018; 175:887–888]. Cell 175:665–678.e23.
50. Watabe-Uchida M, Zhu L, Ogawa SK, Vamanrao A, Uchida N (2012): Whole-brain mapping of direct inputs to midbrain dopamine neurons. Neuron 74:858–873.
51. Menegas W, Bergan JF, Ogawa SK, Isogai Y, Umadevi Venkataraju K, Osten P, *et al.* (2015): Dopamine neurons projecting to the posterior striatum form an anatomically distinct subclass. Elife 4:e10032.
52. Stuber GD, Wise RA (2016): Lateral hypothalamic circuits for feeding and reward. Nat Neurosci 19:198–205.
53. Heise CE, Mitrofanis J (2004): Evidence for a glutamatergic projection from the zona incerta to the basal ganglia of rats. J Comp Neurol 468:482–495.
54. Glangetas C, Fois GR, Jalabert M, Lecca S, Valentinova K, Meye FJ, *et al.* (2015): Ventral subiculum stimulation promotes persistent hyperactivity of dopamine neurons and facilitates behavioral effects of cocaine. Cell Rep 13:2287–2296.
55. Jones RS, Juorio AV, Boulton AA (1983): Changes in levels of dopamine and tyramine in the rat caudate nucleus following alterations in impulse flow in the nigrostriatal pathway. J Neurochem 40:396–401.
56. Centonze D, Usiello A, Gubellini P, Pisani A, Borrelli E, Bernardi G, Calabresi P (2002): Dopamine D2 receptor-mediated inhibition of dopaminergic neurons in mice lacking D2L receptors. Neuropsychopharmacology 27:723–726.
57. Kuzhikandathil EV, Yu W, Oxford GS (1998): Human dopamine D3 and D2L receptors couple to inward rectifier potassium channels in mammalian cell lines. Mol Cell Neurosci 12:390–402.
58. Mercuri NB, Saiardi A, Bonci A, Picetti R, Calabresi P, Bernardi G, Borrelli E (1997): Loss of autoreceptor function in dopaminergic neurons from dopamine D2 receptor deficient mice. Neuroscience 79:323–327.
59. Asif-Malik A, Hoener MC, Canales JJ (2017): Interaction between the trace amine-associated receptor 1 and the dopamine D_2 receptor controls cocaine's neurochemical actions. Sci Rep 7:13901.
60. Espinoza S, Salahpour A, Masri B, Sotnikova TD, Messa M, Barak LS, *et al.* (2011): Functional interaction between trace amine-associated receptor 1 and dopamine D2 receptor. Mol Pharmacol 80:416–425.
61. Lyford GL, Yamagata K, Kaufmann WE, Barnes CA, Sanders LK, Copeland NG, *et al.* (1995): Arc, a growth factor and activity-regulated gene, encodes a novel cytoskeleton-associated protein that is enriched in neuronal dendrites. Neuron 14:433–445.
62. Steward O, Wallace CS, Lyford GL, Worley PF (1998): Synaptic activation causes the mRNA for the IEG Arc to localize selectively near activated postsynaptic sites on dendrites. Neuron 21:741–751.
63. Link W, Konietzko U, Kauselmann G, Krug M, Schwanke B, Frey U, Kuhl D (1995): Somatodendritic expression of an immediate early gene is regulated by synaptic activity. Proc Natl Acad Sci *U S* A 92:5734–5738.
64. Waltereit R, Dammermann B, Wulff P, Scafidi J, Staubli U, Kauselmann G, *et al.* (2001): Arg3.1/Arc mRNA induction by Ca2+ and cAMP requires protein kinase A and mitogen-activated protein kinase/extracellular regulated kinase activation. J Neurosci 21:5484–5493.
65. Tan A, Moratalla R, Lyford GL, Worley P, Graybiel AM (2000): The activity-regulated cytoskeletal-associated protein arc is expressed in different striosome-matrix patterns following exposure to amphetamine and cocaine. J Neurochem 74:2074–2078.
66. Gerfen CR, Paletzki R, Worley P (2008): Differences between dorsal and ventral striatum in Drd1a dopamine receptor coupling of dopamine- and cAMP-regulated phosphoprotein-32 to activation of extracellular signal-regulated kinase. J Neurosci 28:7113–7120.
67. Bertran-Gonzalez J, Bosch C, Maroteaux M, Matamales M, Hervé D, Valjent E, Girault JA (2008): Opposing patterns of signaling activation in dopamine D1 and D2 receptor-expressing striatal neurons in response to cocaine and haloperidol. J Neurosci 28:5671–5685.
68. Kravitz AV, Freeze BS, Parker PR, Kay K, Thwin MT, Deisseroth K, Kreitzer AC (2010): Regulation of parkinsonian motor behaviours by optogenetic control of basal ganglia circuitry. Nature 466:622–626.
69. Grace AA (2016): Dysregulation of the dopamine system in the pathophysiology of schizophrenia and depression. Nat Rev Neurosci 17:524–532.
70. Chen H, Nwe PK, Yang Y, Rosen CE, Bielecka AA, Kuchroo M, *et al.* (2019): A forward chemical genetic screen reveals gut microbiota metabolites that modulate host physiology. Cell 177:1217–1231.e18.
71. Yang W, Munhall AC, Johnson SW (2020): Dopamine evokes a trace amine receptor-dependent inward current that is regulated by AMP kinase in substantia nigra dopamine neurons. Neuroscience 427:77–91.
72. Dave S, Chen L, Yu C, Seaton M, Khodr CE, Al-Harthi L, Hu XT (2019): Methamphetamine decreases K^+ channel function in human fetal astrocytes by activating the trace amine-associated receptor type-1. J Neurochem 148:29–45.
73. Cisneros IE, Ghorpade A (2014): Methamphetamine and HIV-1-induced neurotoxicity: Role of trace amine associated receptor 1 cAMP signaling in astrocytes. Neuropharmacology 85:499–507.
74. Santello M, Toni N, Volterra A (2019): Astrocyte function from information processing to cognition and cognitive impairment. Nat Neurosci 22:154–166.
75. Patel PM, Drummond JC, Cole DJ, Goskowicz RL (1995): Isoflurane reduces ischemia-induced glutamate release in rats subjected to forebrain ischemia. Anesthesiology 82:996–1003.
76. Dubocovich ML (1988): Pharmacology and function of melatonin receptors. FASEB J 2:2765–2773.
77. Scammell TE, Jackson AC, Franks NP, Wisden W, Dauvilliers Y (2019): Histamine: Neural circuits and new medications. Sleep 42:zsy183.
78. Mattucci-Schiavone L, Ferko AP (1985): Acute effects of taurine and a taurine antagonist on ethanol-induced central nervous system depression. Eur J Pharmacol 113:275–278.
79. Cajochen C, Kräuchi K, Wirz-Justice A (2003): Role of melatonin in the regulation of human circadian rhythms and sleep. J Neuroendocrinol 15:432–437.
80. Goonawardena AV, Morairty SR, Dell R, Orellana GA, Hoener MC, Wallace TL, Kilduff TS (2019): Trace amine-associated receptor 1 agonism promotes wakefulness without impairment of cognition in Cynomolgus macaques. Neuropsychopharmacology 44:1485–1493.
81. Schwartz MD, Black SW, Fisher SP, Palmerston JB, Morairty SR, Hoener MC, Kilduff TS (2017): Trace amine-associated receptor 1 regulates wakefulness and EEG spectral composition. Neuropsychopharmacology 42:1305–1314.
82. Yuan XS, Wang L, Dong H, Qu WM, Yang SR, Cherasse Y, *et al.* (2017): Striatal adenosine A_{2A} receptor neurons control active-period sleep via parvalbumin neurons in external globus pallidus. Elife 6:e29055.
83. Izquierdo C, Gómez-Tamayo JC, Nebel JC, Pardo L, Gonzalez A (2018): Identifying human diamine sensors for death related putrescine and cadaverine molecules. PLoS Comput Biol 14: e1005945.